# Journal of Materials Chemistry C

Accepted Manuscript


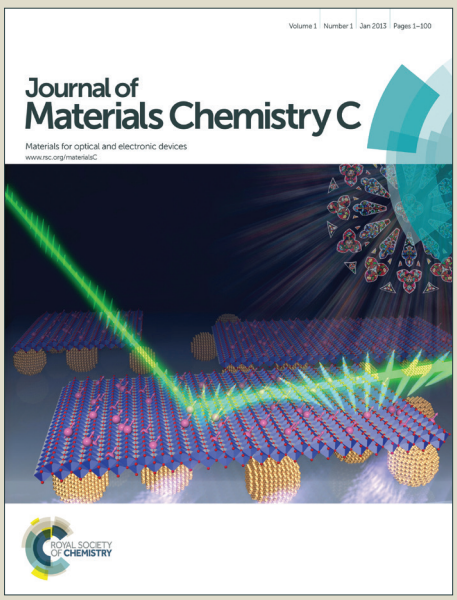



This is an *Accepted Manuscript*, which has been through the Royal Society of Chemistry peer review process and has been accepted for publication.

*Accepted Manuscripts* are published online shortly after acceptance, before technical editing, formatting and proof reading. Using this free service, authors can make their results available to the community, in citable form, before we publish the edited article. We will replace this *Accepted Manuscript* with the edited and formatted *Advance Article* as soon as it is available.

You can find more information about *Accepted Manuscripts* in the Information for Authors.

Please note that technical editing may introduce minor changes to the text and/or graphics, which may alter content. The journal's standard Terms & Conditions and the Ethical guidelines still apply. In no event shall the Royal Society of Chemistry be held responsible for any errors or omissions in this *Accepted Manuscript* or any consequences arising from the use of any information it contains.



ROYAL SOCIETY OF CHEMISTRY

www.rsc.org/materialsC

# Colloidal Silicon Germanium Alloy Nanocrystals with High Boron and Phosphorus Concentration Hydrophilic Shell

*Takashi Kanno, Minoru Fujii*[*]*, Hiroshi Sugimoto, Kenji Imakita*

Department of Electrical and Electronic Engineering, Graduate School of Engineering, Kobe University, Rokkodai, Nada, Kobe, 657-8501, Japan

**Author Information**

Corresponding Author

[*]E-mail: fujii@eedept.kobe-u.ac.jp. Telephone: +81-78-803-6081

Journal of Materials Chemistry C Accepted Manuscript

**Abstract**

$Si_{1-x}Ge_x$ alloy nanocrystals potentially have superior properties compared to Si nanocrystals such as the enhanced absorption cross-section and wider controllability of the band gap energy. However, reports on the synthesis of $Si_{1-x}Ge_x$ alloy nanocrystals, especially colloidal $Si_{1-x}Ge_x$ alloy nanocrystals, are still very limited and the quality is not as high as that of colloidal Si nanocrystals. Here, we report the development of a new type of luminescing colloidal $Si_{1-x}Ge_x$ alloy nanocrystals 3 to 6 nm in diameters. The characteristic feature of the $Si_{1-x}Ge_x$ alloy nanocrystals is the formation of high B and P concentration layers on the surface. The shell acts as inorganic atomic ligands and B and P codoped $Si_{1-x}Ge_x$ nanocrystals can be dispersed in alcohol without any surface functionalization processes.

**Graphical table of contents**


**Keywords** silicon, germanium, alloy nanocrystals, impurity doping, colloids

Journal of Materials Chemistry C Accepted Manuscript

## 1. Introduction

Colloidal semiconductor nanocrystals (NCs) have been attracting significant attention as precursors for printable optoelectronic devices[1–7] and for biological applications.[8–10] In particular, the research on Si NCs is growing rapidly because of the non-toxicity as a chemical element and the high compatibility with the standard semiconductor device technology.[11–14] The band gap energy of Si NCs can be controlled from the bulk band gap (1.12 eV) to the visible range by the size.[15,16] A drawback of Si NCs as an optical material is the small absorption cross-section in the visible and near infrared (NIR) range due to the indirect band gap nature of the energy band structure.[17] A promising approach to overcome the problem is the alloying with Ge, *i.e.*, the formation of $Si_{1-x}Ge_x$ alloy NCs.[18] By controlling the composition and the size simultaneously, the absorption cross-section in the visible to NIR range can be enhanced.[19,20] Furthermore, the controllable range of the band gap can be extended below the bulk Si band gap, which is important for the utilization of low-energy photons in photovoltaic applications. $Si_{1-x}Ge_x$ NCs are also known to have large thermoelectric figure of merit.[21–23]

Despite the attractive properties, however, research on $Si_{1-x}Ge_x$ NCs, especially colloidal form ones, is still very limited. Recently, Pi *et al*.[24] produced free-standing $Si_{1-x}Ge_x$ alloy NCs, exhibiting photoluminescence (PL) at 1.5 eV by non-thermal plasma decomposition of silane and germane.[25,26] Yasar-Inceoglu *et al.* applied a similar process and produced $Si_{1-x}Ge_x$ alloy NCs smaller than 10 nm with good controllability over a wide alloy composition.[27] Erogbogbo *et al*. produced colloidal solution of $Si_{1-x}Ge_x$ NCs (15 to 30 nm in diameter) by ultrasonication of the powder produced by laser pyrolysis of silane and germane in benzonitrile and acetonitrile.[28] Barry *et al*. grew $Si_{1-x}Ge_x$ NCs in solid matrices by annealing the mixture of hydrogensilsesquioxane (HSQ) and $GeI_2$ and extracted them by HF etching.[29] They

Journal of Materials Chemistry C Accepted Manuscript

functionalized the NC surface by 1-dodecene to disperse them in hexane and observed the PL at 1.4-1.5 eV with high quantum yields (16 ± 3%), although the uniformity of the samples was not very high, *i.e.*, the samples were a mixture of Si-rich (diameter: 3-14 nm) and Ge-rich (diameter: 9-22 nm) NCs.

In this work, we report the development of a new type of colloidal $Si_{1-x}Ge_x$ NCs ($0 \leq x \leq 0.48$) stable in polar solvents for a long period without organic capping by the formation of a high B and P concentration layer on the surface. The high B and P concentration shell induces negative potential on the surface and makes $Si_{1-x}Ge_x$ NCs dispersible in polar solvents due to the electrostatic repulsion without any functionalization processes. We show that the colloidal solution of B and P codoped $Si_{1-x}Ge_x$ NCs is scattering-free and very clear in a wide composition range, and the optical band gap and the luminescence energy can be controlled in a wide range by the composition and the size.

## 2. Experimental section

For the preparation of B and P codoped colloidal $Si_{1-x}Ge_x$ NCs, borophosphosilicate glass (BPSG) films containing B and P codoped $Si_{1-x}Ge_x$ NCs were first prepared on stainless steel plates as follows. Si, Ge, $SiO_2$, $B_2O_3$ and $P_2O_5$ were simultaneously sputter-deposited in Ar gas ($2x10^{-2}$ Torr) by a single target rf magnetron sputtering apparatus (ANELVA SPF-210H). The composition of the films was controlled by changing the area ratio of the materials composing the sputtering target. The films were then peeled from the plates and flakes of the films were corrected. The flakes were then annealed in a $N_2$ gas atmosphere for 30 min at temperatures from 1050 to 1150°C to grow B and P codoped $Si_{1-x}Ge_x$ NCs in BPSG matrices. To etch out BPSG matrices and isolate codoped $Si_{1-x}Ge_x$ NCs, the flakes were dissolved in HF solution (46 wt%)

Journal of Materials Chemistry C Accepted Manuscript

for 1 hr at 25°C. In this etching condition, BPSG matrices are completely etched out. Isolated $Si_{1-x}Ge_x$ NCs were separated from HF solution by centrifugation (4000 rpm, 1 min) in an ultrafiltration concentrator (VS0202: Sartorius Stedim Biotech GmbH), and $Si_{1-x}Ge_x$ NC powder was obtained in the concentrator. Methanol was then added to the concentrator to disperse $Si_{1-x}Ge_x$ NCs in methanol. The procedure was repeated more than 10 times to remove HF completely. In methanol, a majority of $Si_{1-x}Ge_x$ NCs are dispersed, while a small fraction of them form agglomerates and precipitate. Precipitates were removed by centrifugation (4000 rpm, 2 min), and only a supernatant liquid was stored in a vial. As will be shown later, the supernatant liquid was very clear and precipitates were no more formed for more than 6 months. All the processes were performed in an ordinary laboratory environment.

The composition of B and P codoped colloidal $Si_{1-x}Ge_x$ NCs was obtained by inductively coupled plasma atomic emission spectroscopy (ICP-AES) (SII SPS3100). For the ICP-AES measurements, solution was changed from methanol to distilled water by a fractional process. The size of NCs was estimated by TEM observations (HITACHI H-7000, JEOL JEM-2010). The optical transmittance spectra of colloidal solutions were acquired by a spectrophotometer (Shimadzu UV-3101PC). PL spectra were measured by a scanning monochromator equipped with a photomultiplier and a liquid-$N_2$ cooled InGaAs NIR photodiode (Horiba Fluorolog-3). The excitation source was a monochromatized Xe lamp (405 nm). For a few samples with weak PL intensity, PL was excited by a 405 nm semiconductor laser and detected by a liquid-$N_2$ cooled InGaAs diode array (Roper Scientific OMA-V-SE). The spectral response of the detection system was corrected with the reference spectrum of a standard halogen lamp. The samples for XPS (ULVAC-PHI phi X-tool) and Raman measurements were prepared by dropping colloidal solutions onto Au-coated Si wafers. The X-ray source was Al Kα. Raman

Journal of Materials Chemistry C Accepted Manuscript

spectra were obtained by a micro-Raman setup (50X objective lens, NA: 0.8). The excitation source was 514.5 nm light from an Ar ion laser. The excitation power was about 1 mW. All the measurements were carried out at room temperature.

## 3. Results and discussion

The list of the samples studied is shown in Table 1. Hereafter, we refer a sample by the name designated in the left-most column of the table. The number in a sample name represents the annealing temperature (°C), while the symbols A to D classify the composition of the sputtering target. From A to D, the area ratio of Ge in the sputtering target increases.

**Table 1** List of samples: $T_a$: annealing temperature, Ge/(Si+Ge): Ge composition (ICP-AES), $C_B$ and $C_P$: B and P atomic concentration (ICP-AES), $d$: NC diameter (TEM), σ: standard deviation (TEM), $E_{opt}$: optical band gap.

| Sample | $T_a$ (°C) | Ge/(Si+Ge) | $C_B$ (at%) | $C_P$ (at%) | $d$ (nm) | σ (nm) | $E_{opt}$ (eV) |
|---|---|---|---|---|---|---|---|
| A1050 | 1050 | 0.017 | 31.76 | 4.97 | N/A | N/A | 2.08 |
| A1100 | 1100 | 0.028 | 34.17 | 5.55 | 3.64 | 0.55 | 1.70 |
| A1150 | 1150 | 0.026 | 31.58 | 6.42 | 4.69 | 0.97 | 1.51 |
| B1050 | 1050 | 0.091 | 27.21 | 6.51 | 3.40 | 0.68 | 1.66 |
| B1100 | 1100 | 0.080 | 27.76 | 6.10 | 3.73 | 0.68 | 1.53 |
| B1150 | 1150 | 0.085 | 25.34 | 6.43 | 5.28 | 1.1 | 1.38 |
| C1050 | 1050 | 0.204 | 20.56 | 5.25 | 3.68 | 0.68 | 1.65 |
| C1100 | 1100 | 0.195 | 22.39 | 4.51 | 4.02 | 0.69 | 1.51 |

Journal of Materials Chemistry C Accepted Manuscript

| | | | | | | | |
|---|---|---|---|---|---|---|---|
| C1150 | 1150 | 0.218 | 22.13 | 6.00 | 5.27 | 1.28 | 1.29 |
| D1100 | 1100 | 0.469 | 15.08 | 4.17 | 5.35 | 1.26 | 1.20 |
| D1150 | 1150 | 0.480 | 14.54 | 5.41 | 5.67 | 2.53 | 1.08 |

Fig. 1a shows photographs of colloidal solutions (methanol) in which $Si_{1-x}Ge_x$ NCs prepared with different conditions are dispersed. We can see yellowish to dark-brownish clear solutions. The color becomes dense with increasing the Ge composition and annealing temperature. Fig. 1b and c shows Ge composition and annealing temperature, respectively, dependence of the transmission spectra. The transmittance is higher than 90% in the NIR range even for the sample with the highest Ge composition. This indicates that light scattering by agglomerates is negligibly small and NCs are well-dispersed in solution.

Fig. 1d shows annealing temperature dependence of the optical band gaps ($E_{opt}$) estimated by the Tauc plot of absorption spectra, $(\alpha h\nu)^{1/2} = B(h\nu - E_{opt})$, where $\alpha$ is the absorption coefficient, $h$ is the Plank's constant and $\nu$ is the photon frequency. In Fig. 1e, $E_{opt}$ is plotted as a function of NC size estimated from TEM images described later. $E_{opt}$ depends both on the Ge composition and the annealing temperature and is changed in a very wide range (1.1-2.1 eV).

Journal of Materials Chemistry C Accepted Manuscript

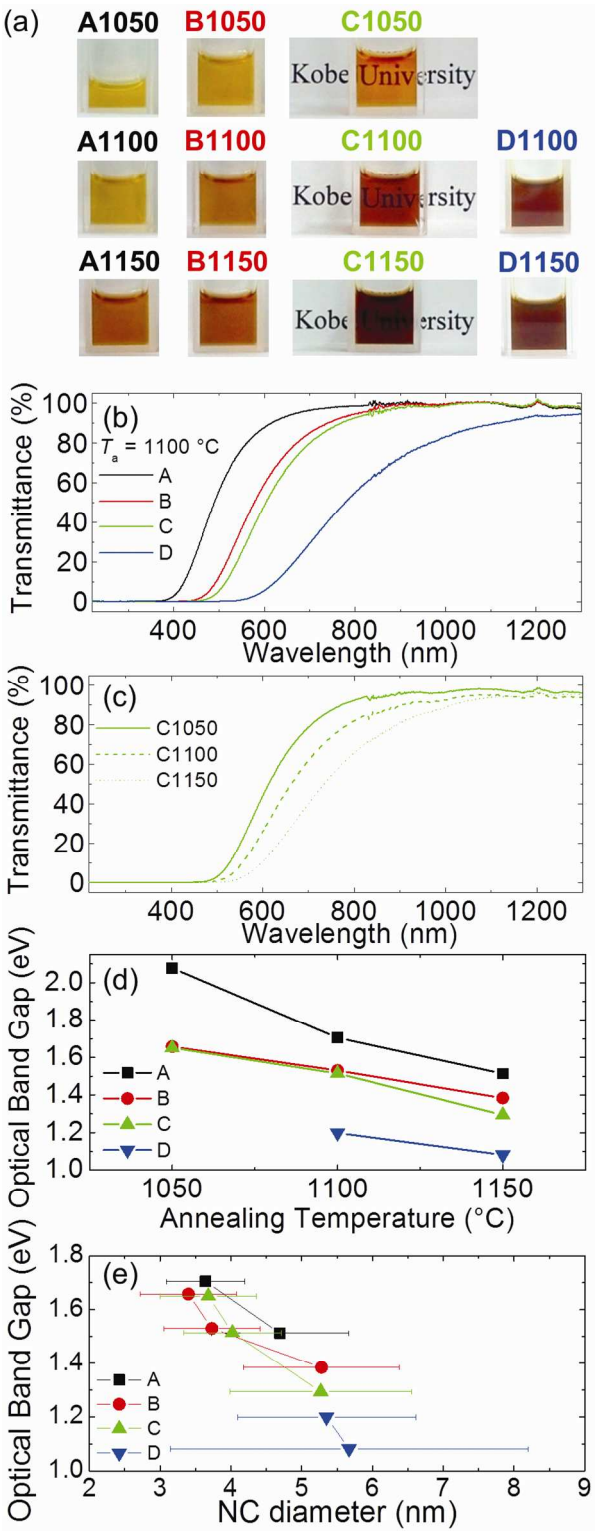


**Fig. 1** (a) Photographs of B and P codoped colloidal $Si_{1-x}Ge_x$ NCs (methanol solution). Annealing temperature and Ge composition are changed. (b) Ge composition dependence of

Journal of Materials Chemistry C Accepted Manuscript

transmittance spectra ($T_a$=1100°C). (c) Annealing temperature dependence of transmittance spectra. The Ge composition is fixed. Optical band gap as a function of (d) annealing temperature and (e) NC diameter for four series of samples.

Fig. 2a and b shows TEM images of codoped $Si_{1-x}Ge_x$ NCs prepared by annealing at 1100 (C1100) and 1150°C (C1150), respectively. NCs are isolated on C-coated Cu meshes and no three-dimensional aggregates are observed. This is consistent with the high optical transmittance in the NIR region in Fig. 1b. The NCs are assigned to diamond structure $Si_{1-x}Ge_x$ alloy crystal from the electron diffraction patterns. High-resolution TEM observations reveal that almost all NCs are single crystal.

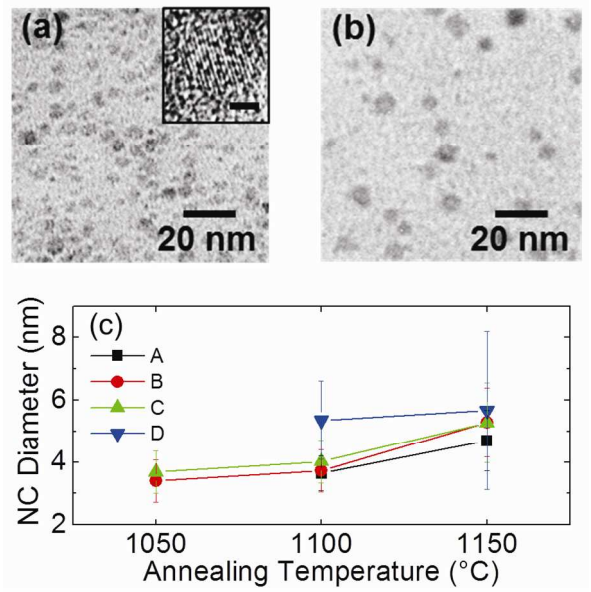


**Fig. 2** TEM images of B and P codoped $Si_{1-x}Ge_x$ NCs: (a) C1100, (b) C1150. (inset: High-resolution TEM image, the scale bar represents 2 nm). (c) Diameter of $Si_{1-x}Ge_x$ NCs estimated from TEM images as a function of annealing temperature.

Journal of Materials Chemistry C Accepted Manuscript

The average diameters of nanocrystals (*d*) estimated from TEM images are summarized in Table 1 and plotted in Fig. 2c. The error bars represents the standard deviation (σ) of the size distribution. The diameter increases with increasing the annealing temperature similar to the case of B and P codoped Si NCs.[30] The diameter also increases with increasing Ge composition. This may be due to larger diffusion coefficient of Ge atoms in BPSG matrices than Si atoms during annealing.

Figure 3a-d shows the Raman spectra obtained by drop-coating the solution on Au-coated Si wafers. In low Ge concentration samples, *e.g.*, sample series A (Fig. 3a), a peak assigned to Si–Si bonds is observed around 520 $cm^{-1}$. The peak is very broad with a long tail toward lower wavenumber. The peak becomes sharp with increasing the annealing temperature. In higher Ge composition samples, broad peaks due to Si–Ge and Ge–Ge bonds appear around 400 and 280 $cm^{-1}$, respectively. In the highest Ge composition samples (sample series D (Fig. 3d)), the intensities of the three bands are comparable. The spectral shape with the Ge–Ge, Si–Ge and Si–Si bands is typical of $Si_{1-x}Ge_x$ alloy[31–33] and is a direct evidence that the samples are not the mixture of Si and Ge NCs, but $Si_{1-x}Ge_x$ alloy NCs. The Si–Si peak shifts to lower wavenumber with increasing Ge composition and reaches 494 $cm^{-1}$, when the Ge composition is the highest. The Ge composition dependence of the wavenumber of the Si–Si peak agrees well with those reported for $Si_{1-x}Ge_x$ alloy[31–33] (see Figure S1 in supplementary information). This is another direct evidence that $Si_{1-x}Ge_x$ alloy NCs are formed. Compared to bulk $Si_{1-x}Ge_x$ alloy, the peaks are much broader. The broadening is considered to be due to small size of NCs and heavy doping of B and P.

Journal of Materials Chemistry C Accepted Manuscript

From the data in Figs. 1-3, we can conclude that $Si_{1-x}Ge_x$ alloy NCs are formed and they can be well-dispersed in methanol without any surface functionalization processes. It should be stressed here that without B and P codoping, $Si_{1-x}Ge_x$ alloy NCs form agglomerates in methanol and precipitate to the bottom of a vial. Therefore, it is clear that B and P codoping plays a crucial role for the high solution dispersibility of $Si_{1-x}Ge_x$ alloy NCs.

In B and P codoped Si NCs, the solution was very stable for more than years.[30] Similarly, codoped $Si_{1-x}Ge_x$ NCs do not form agglomerates and the solutions are clear for more than 6 months. However, in contrast to codoped Si NCs, the color becomes slightly thin for the first one month after preparation. This is probably due to oxidation of the surface and etching of the Ge–O bonds in methanol. After about one month from preparation, change of the color is almost not observed.

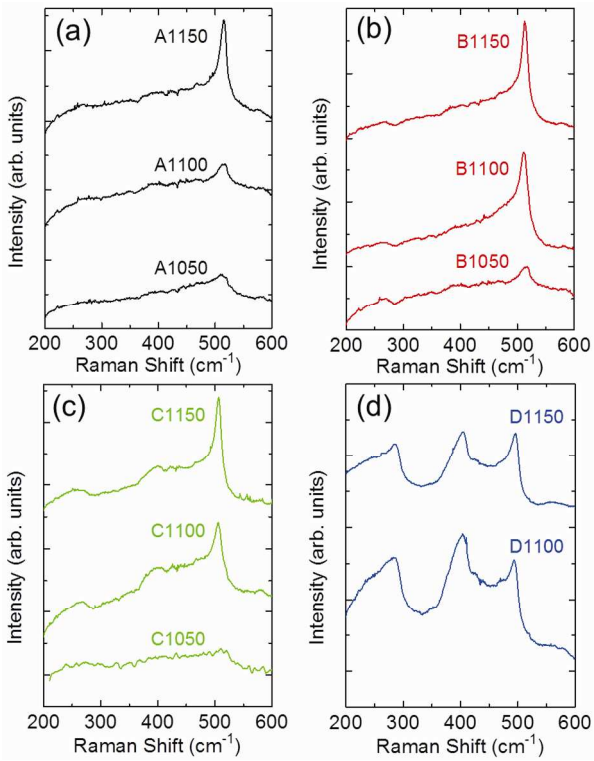


Journal of Materials Chemistry C Accepted Manuscript

**Fig. 3** Raman spectra of B and P codoped $Si_{1-x}Ge_x$ NCs with different Ge composition ratio.

In order to study the surface structure of $Si_{1-x}Ge_x$ NCs and understand the mechanism of the high solution dispersibility, we measure X-ray photoelectron spectroscopy (XPS). Fig. 4a shows the XPS spectra of 2p core electrons of Si. The Si 2p peak shifts from 99.3 to 104 eV depending on the five oxidation states, *i.e.*, $Si^{0+}$, $Si^{+}$, $Si^{2+}$, $Si^{3+}$ and $Si^{4+}$.[34] In Fig. 4a, we can see two peaks corresponding to $Si^{0+}$ and $Si^{4+}$ for all the samples. The $Si^{4+}$ peak arises from Si dioxide formed on the surface during storage in methanol and/or in air for XPS measurements and the $Si^{0+}$ peak from Si NC cores. In the figure, the intensity ratio ($Si^{0+}/Si^{4+}$) increases with increasing the Ge composition and the annealing temperature. This is explained by the increase of the size and resultant decrease of the surface to volume ratio. Similar dependence is observed in the Ge 3d XPS spectra (Fig. 4b) and it is probably explained by the same mechanism.

Journal of Materials Chemistry C Accepted Manuscript

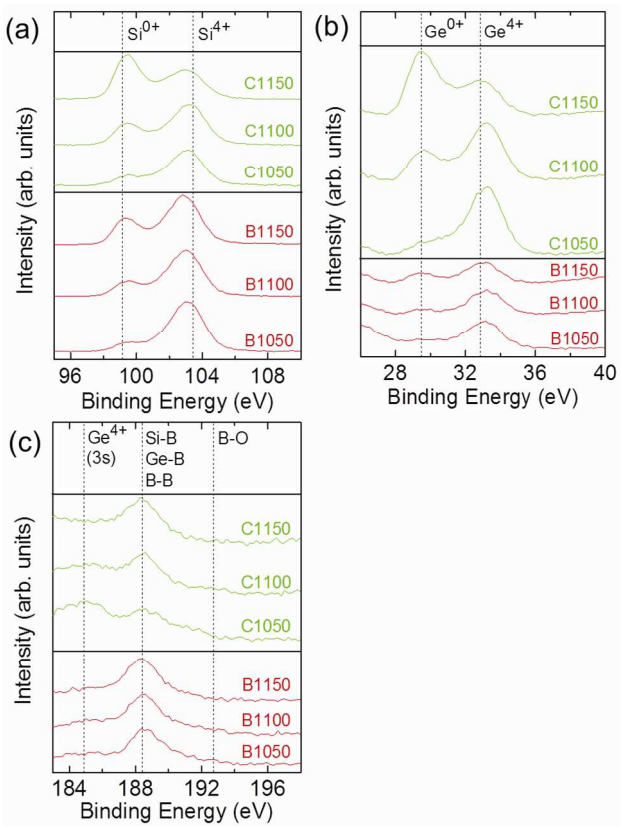


**Fig. 4** XPS spectra of P and B codoped $Si_{1-x}Ge_x$ NCs. (a) Si 2p, (b) Ge 3d, (c) B 1s.

Fig. 4c shows the B 1s XPS spectra. In contrast to the Si 2p and Ge 3d peaks, the signal from non-oxidized B atoms is much larger than that of oxidized B atoms.[35] In fact, the signal from oxidized B atoms is almost undetectable. B concentration estimated from ICP-AES measurements is several tenth of at% (Table 1). This concentration is much larger than the solid solubility of B atoms in $Si_{1-x}Ge_x$ crystal. Therefore, majority of B atoms are considered to exist on the surface of $Si_{1-x}Ge_x$ NCs in the non-oxidized states. Unfortunately, in B and P codoped $Si_{1-x}Ge_x$ NCs, the P 2p XPS signals cannot be distinguished due to strong signals from Ge $3p_{1/2}$, $3p_{3/2}$. However, considering very high P concentration (3-5 at%, Table 1) and from the analogy of the XPS data of B and P codoped Si NCs,[36,37] it is very plausible that a large part of P atoms exist

Journal of Materials Chemistry C Accepted Manuscript

also on the surface of NCs in the non-oxidized states. We believe that high B and P concentration layers on the surface of $Si_{1-x}Ge_x$ NCs make the surface potential negative and prevent the agglomeration of NCs in polar solvents.

One of the advantages of $Si_{1-x}Ge_x$ NCs compared to Si NCs is the enhanced absorption cross section. Fig. 5 shows per-atom absorption cross-sections of B and P codoped colloidal $Si_{1-x}Ge_x$ NCs at selected energies, 4.1, 3.1 and 1.8 eV, respectively, as a function of NC size (see Fig. S1 for per-atom absorption cross-section spectra). Solid squares, circles, triangles and inverted triangles correspond to sample series A, B, C and D, respectively. As references, the data reported for Si (open left-pointing triangles)[38] and Ge (open right-pointing triangles)[39] NCs prepared by a non-thermal plasma synthesis process are shown. In all three energies, the absorption cross-sections depend not only on the size, but also on the Ge composition. It increases significantly with increasing the Ge composition at the same NC sizes.

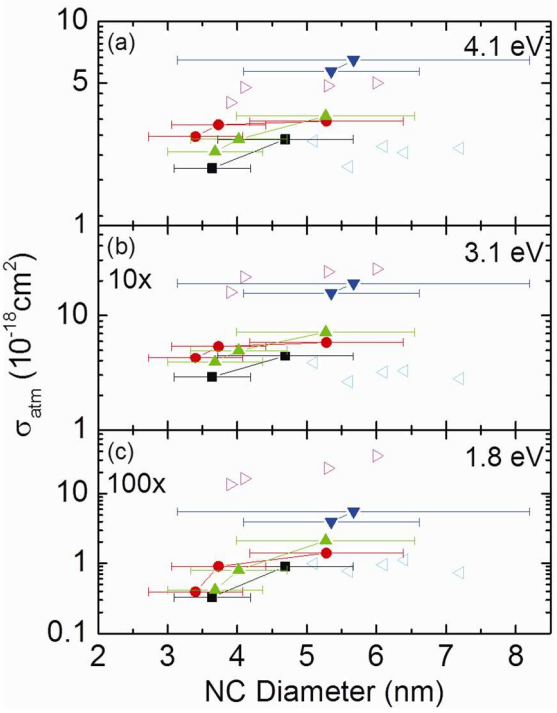


Journal of Materials Chemistry C Accepted Manuscript

**Fig. 5** Plot of per-atom absorption cross-sections of B and P codoped $Si_{1-x}Ge_x$ NCs at (a) 4.1, (b) 3.1 and (c) 1.8 eV as a function of NC diameter. Solid squares, circles, triangles and inverted triangles correspond to sample series A, B, C and D, respectively. Open left-pointing triangles and right-pointing triangles are the data of Si NCs[38] and Ge NCs[39] synthesized from non-thermal plasma synthesis process.

Fig. 6a shows normalized PL spectra of B and P codoped $Si_{1-x}Ge_x$ NCs annealed at 1100°C at room temperature. PL spectra of other samples are shown in the supplemental material (Fig. S2). We can see a broad PL peak in the NIR region. The peak shifts to lower energy with increasing the Ge composition. The reports on the observation of Ge composition dependent PL shift in colloidal $Si_{1-x}Ge_x$ NC have been very limited.[29] In Fig. 6b, the PL peak energy is plotted as a function of $T_a$ for sample series A to D. The PL energy depends on $T_a$ as well as on the Ge composition, and by these parameters, it is controlled from 1.43 to 0.98 eV. To our knowledge, this is the lowest PL energy achieved in colloidal $Si_{1-x}Ge_x$ NCs.

Fig. 6c shows the relation between the PL peak energy and the diameter of NCs. The PL peak energy decreases with increasing the diameter. Furthermore, in many cases, the PL peak energy of samples with smaller Ge composition is larger than those with larger Ge composition when the size is similar, although there are a few exceptions probably due to relatively large size distributions.

Journal of Materials Chemistry C Accepted Manuscript

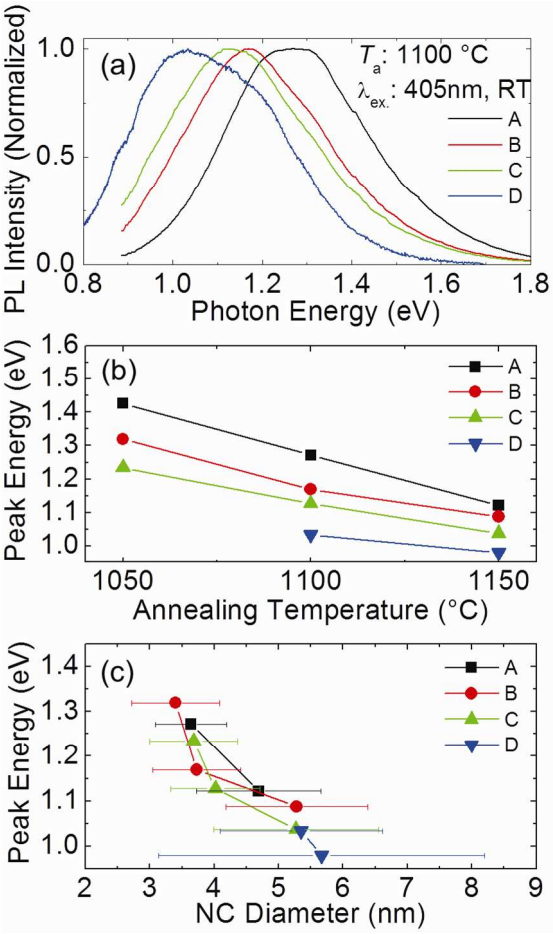


**Fig. 6** (a) Normalized PL spectra of B and P codoped $Si_{1-x}Ge_x$ NCs annealed at 1100°C. (b) PL peak energy as a function of annealing temperature for 4 series of samples. (c) Relation between PL peak energy and NC diameter for 4 series of samples.

In B and P codoped Si NCs, the size dependence of the PL peak energy is studied in detail and the peak energy is reported to be 300-400 meV smaller than those of undoped Si NCs.[30,40] The low-energy PL is considered to be due to the electronic transition between donor and acceptor states. Similarly, in B and P codoped $Si_{1-x}Ge_x$ NCs, the PL is considered to arise from donor-acceptor pairs when the Ge composition is small. However, when Ge composition increases, it is

Journal of Materials Chemistry C Accepted Manuscript

not clear whether B and P are doped in the substitutional sites of $Si_{1-x}Ge_x$ NCs or not and thus the PL origin cannot be identified at this stage of research.

In the present work, the largest Ge composition is 0.48 ($Si_{0.52}Ge_{0.48}$). In principle, the present method can be applied to a larger Ge composition range and even to Ge NCs. However, long term stability in solution becomes worse with increasing Ge composition. Furthermore, PL quantum yield decreases and the PL is hardly observed above the concentration. This suggests that stable high B and P concentration shells are not formed at higher Ge composition ranges.

## 4. Conclusions

We have succeeded in fabricating $Si_{1-x}Ge_x$ alloy NCs ($0 \leq x \leq 0.48$) dispersible in polar solvents without any surface functionalization processes. The characteristic structural feature of the $Si_{1-x}Ge_x$ NCs is the formation of high B and P concentration layers on the surface, which make $Si_{1-x}Ge_x$ NCs hydrophilic. The codoped $Si_{1-x}Ge_x$ NCs exhibited PL in the NIR range and the PL energy as well as the optical band gap can be controlled in wide ranges by the size and the Ge composition. We also demonstrated that the optical absorption cross-section is significantly enhanced compared to that of Si NCs with comparable sizes.

## Acknowledgements

This work is supported by KAKENHI (23310077, 24651143).

## Notes and references

Journal of Materials Chemistry C Accepted Manuscript

1. D. V. Talapin and C. B. Murray, *Science*, 2005, **310**, 86–89.

2. J. J. Urban, D. V. Talapin, E. V. Shevchenko, C. R. Kagan, and C. B. Murray, *Nat. Mater.*, 2007, **6**, 115–121.

3. J. Zhao, J. A. Bardecker, A. M. Munro, M. S. Liu, Y. Niu, I.-K. Ding, J. Luo, B. Chen, A. K.-Y. Jen, and D. S. Ginger, *Nano Lett.*, 2006, **6**, 463–467.

4. J. Kwak, W. K. Bae, D. Lee, I. Park, J. Lim, M. Park, H. Cho, H. Woo, D. Y. Yoon, K. Char, S. Lee, and C. Lee, *Nano Lett.*, 2012, **12**, 2362–2366.

5. J. M. Luther, M. Law, M. C. Beard, Q. Song, M. O. Reese, R. J. Ellingson, and A. J. Nozik, *Nano Lett.*, 2008, **8**, 3488–3492.

6. K. S. Leschkies, T. J. Beatty, M. S. Kang, D. J. Norris, and E. S. Aydil, *ACS Nano*, 2009, **3**, 3638–3648.

7. S. A. McDonald, G. Konstantatos, S. Zhang, P. W. Cyr, E. J. D. Klem, L. Levina, and E. H. Sargent, *Nat. Mater.*, 2005, **4**, 138–142.

8. X. Michalet, F. F. Pinaud, L. A. Bentolila, J. M. Tsay, S. Doose, J. J. Li, G. Sundaresan, A. M. Wu, S. S. Gambhir, and S. Weiss, *Science*, 2005, **307**, 538–544.

9. I. L. Medintz, M. H. Stewart, S. A. Trammell, K. Susumu, J. B. Delehanty, B. C. Mei, J. S. Melinger, J. B. Blanco-Canosa, P. E. Dawson, and H. Mattoussi, *Nat. Mater.*, 2010, **9**, 676–684.

10. W. Cai, D.-W. Shin, K. Chen, O. Gheysens, Q. Cao, S. X. Wang, S. S. Gambhir, and X. Chen, *Nano Lett.*, 2006, **6**, 669–676.

11. M. C. Beard, K. P. Knutsen, P. Yu, J. M. Luther, Q. Song, W. K. Metzger, R. J. Ellingson, and A. J. Nozik, *Nano Lett.*, 2007, **7**, 2506–2512.

12. J. B. Miller, A. R. Van Sickle, R. J. Anthony, D. M. Kroll, U. R. Kortshagen, and E. K. Hobbie, *ACS Nano*, 2012, **6**, 7389–7396.

13. M. L. Mastronardi, F. Maier-Flaig, D. Faulkner, E. J. Henderson, C. Kübel, U. Lemmer, and G. A. Ozin, *Nano Lett.*, 2012, **12**, 337–342.

14. C. M. Hessel, D. Reid, M. G. Panthani, M. R. Rasch, B. W. Goodfellow, J. Wei, H. Fujii, V. Akhavan, and B. A. Korgel, *Chem. Mater.*, 2012, **24**, 393–401.

15. Y. Kanzawa, T. Kageyama, S. Takeoka, M. Fujii, S. Hayashi, and K. Yamamoto, *Solid State Commun.*, 1997, **102**, 533–537.

16. S. Takeoka, M. Fujii, and S. Hayashi, *Phys. Rev. B*, 2000, **62**, 16820–16825.

Journal of Materials Chemistry C Accepted Manuscript

17. D. Kovalev, H. Heckler, G. Polisski, and F. Koch, *Phys. Status Solidi B*, 1999, **215**, 871–932.

18. S. Takeoka, K. Toshikiyo, M. Fujii, S. Hayashi, and K. Yamamoto, *Phys. Rev. B*, 2000, **61**, 15988–15992.

19. R. Braunstein, A. R. Moore, and F. Herman, *Phys. Rev.*, 1958, **109**, 695–710.

20. R. Hull, J. C. Bean, R. K. Willardson, and E. R. Weber, *Germanium Silicon: Physics and Materials*, Academic Press, San Diego, CA, 1999.

21. B. Yu, M. Zebarjadi, H. Wang, K. Lukas, H. Wang, D. Wang, C. Opeil, M. Dresselhaus, G. Chen, and Z. Ren, *Nano Lett.*, 2012, **12**, 2077–2082.

22. Z. Zamanipour, X. Shi, A. M. Dehkordi, J. S. Krasinski, and D. Vashaee, *Phys. Status Solidi A*, 2012, **209**, 2049–2058.

23. Y. Lan, A. J. Minnich, G. Chen, and Z. Ren, *Adv. Funct. Mater.*, 2010, **20**, 357–376.

24. X. D. Pi and U. R. Kortshagen, *Nanotechnology*, 2009, **20**, 295602.

25. L. Mangolini, E. Thimsen, and U. R. Kortshagen, *Nano Lett.*, 2005, **5**, 655–659.

26. R. Gresback, Z. Holman, and U. R. Kortshagen, *Appl. Phys. Lett.*, 2007, **91**, 093119.

27. O. Yasar-Inceoglu and L. Mangolini, *Mater. Lett.*, 2013, **101**, 76–79.

28. F. Erogbogbo, T. Liu, N. Ramadurai, P. Tuccarione, L. Lai, M. T. Swihart, and P. N. Prasad, *ACS Nano*, 2011, **5**, 7950–7959.

29. S. D. Barry, Z. Yang, J. A. Kelly, E. J. Henderson, and J. G. C. Veinot, *Chem. Mater.*, 2011, **23**, 5096–5103.

30. H. Sugimoto, M. Fujii, K. Imakita, S. Hayashi, and K. Akamatsu, *J. Phys. Chem. C*, 2013, **117**, 11850–11857.

31. M. A. Renucci, J. B. Renucci, and M. Cardona, in *Proceedings of the second International Conference on Light Scattering in Solids*, ed. M. Balkanski, Flammarion, Paris, 1971, pp. 326–329.

32. M. I. Alonso and K. Winer, *Phys. Rev. B*, 1989, **39**, 10056–10062.

33. J. C. Tsang, P. M. Mooney, F. Dacol, and J. O. Chu, *J. Appl. Phys.*, 1994, **75**, 8098–8108.

34. S. M. A. Durrani, M. F. Al-Kuhaili, and E. E. Khawaja, *J. Phys.: Condens. Matter*, 2003, **15**, 8123–8135.

Journal of Materials Chemistry C Accepted Manuscript

35. A. V. Naumkin, A. Kraut-Vass, S. W. Gaarenstroom, and C. J. Powell, *NIST Standard Reference Database 20, Version 4.1 (web version) (http://srdata.nist.gov/xps/).*, 2012.

36. H. Sugimoto, M. Fujii, K. Imakita, S. Hayashi, and K. Akamatsu, *J. Phys. Chem. C*, 2013, **117**, 6807–6813.

37. M. Fujii, H. Sugimoto, M. Hasegawa, and K. Imakita, *J. Appl. Phys.*, 2014, **115**, 084301.

38. R. Gresback, Y. Murakami, Y. Ding, R. Yamada, K. Okazaki, and T. Nozaki, *Langmuir*, 2013, **29**, 1802–1807.

39. Z. C. Holman and U. R. Kortshagen, *Appl. Phys. Lett.*, 2012, **100**, 133108.

40. H. Sugimoto, M. Fujii, K. Imakita, S. Hayashi, and K. Akamatsu, *J. Phys. Chem. C*, 2012, **116**, 17969–17974.

Journal of Materials Chemistry C Accepted Manuscript